Ethanol Oxidation on Pd/Au(111) Bimetallic Surfaces in Alkaline Solution

Milutin Smiljanić[1], Zlatko Rakočević[1], Svetlana Štrbac[2,*

[1] INS Vinča, Laboratory of Atomic Physics, University of Belgrade, Mike Alasa 12-14, 11001 Belgrade, Serbia
[2] ICTM-Institute of Electrochemistry, University of Belgrade, Njegoševa 12, 11000 Belgrade, Serbia
*E-mail: sstrbac@tmf.bg.ac.rs

Catalytic properties of Pd/Au(111) nanostructures obtained by spontaneous palladium deposition using $PdSO_4$ and $PdCl_2$ salts were examined for the oxidation of ethanol in alkaline media. Atomic force microscopy has shown that counter anions in Pd salts are responsible for the differences in surface topography. In both cases the oxidation of ethanol is characterized by the rise of a new peak at approximately the same potential for the same coverage, indicating similar electronic modification of Pd islands by the Au(111) substrate. Pd/Au(111) nanostructures obtained using $PdCl_2$ salt have shown higher ethanol oxidation current densities, which can be ascribed to the surface structure consisting of thinner and smoother Pd deposit providing more convenient sites for the adsorption of ethanol and its subsequent oxidation.

Keywords: Ethanol oxidation, palladium, Au(111), AFM, alkaline solution

1. INTRODUCTION

Direct alcohol fuel cells have attracted much attention in recent years because of high conversion efficiency, high power density, low pollution and a wide range of applications. Ethanol as a fuel has shown some advantages over other alcohols, particularly methanol, due to less toxicity and due to its availability as the product of the fermentation of renewable biomass resources [1]. It is well established that ethanol oxidation occurs mainly via two reaction mechanisms, so called C_1 and C_2 mechanisms. CO_2 as a desired oxidation product is obtained in C_1 mechanism, followed with the exchange of 12 e- per ethanol molecule and maximum energy recovery. In C_2 mechanism only partial oxidation occurs, and ethanol is converted to acetaldehyde and finally to acetic acid or acetate ions [2–4]. It should be emphasized that the breaking of C–C bond and the oxidation of the adsorbed particles occur more easily in alkaline than in acidic media [5,6]. Recently, alkaline direct alcohol fuel cells are

receiving an increased attention due to the advances in tailoring alkaline membranes that conduct hydroxide ions [7]. Another advantage of alkaline over acidic solutions is the improved stability of electrocatalyst.

While the main product of ethanol oxidation on gold electrodes in acid solutions is acetaldehyde [4, 8], in alkaline solutions it could be further oxidized to acetic acid as proved using both electrochemical and spectroscopic techniques [2–4]. It is shown that the reaction proceeds through C_2 mechanism and that acetic acid (acetate ion) is the only product detected [4]. Similar activity of carbon nanotubes supported huge gold nanoparticles [9] as well as of carbon supported Au nanoparticles for ethanol oxidation in alkaline media is recently reported [10]. On the other hand, pure polycrystalline Pd, Pd(poly) [11,12], and various Pd based electrodes exhibit high catalytic activity for ethanol oxidation in alkaline solutions, even better than Pt based electrodes in terms of activity and poison tolerance [13–17]. Mechanism of ethanol oxidation on polycrystalline Pd [11,12] is highly dependent on the electrolyte pH and ethanol concentration. The best performance is achieved for pH=14 with the acetate as the main product, as shown by in situ FTIR spectroscopic measurements. The C-C bond cleavage of ethanol occurred with the formation of CO_2 at pH<= 13, but with a quite low activity. No CO formation was detected during the oxidation of ethanol on Pd indicating that the process is non-poisoning one.

Pd/Au bimetallic catalysts obtained by various methods are extensively explored as improved electrode materials for ethanol oxidation. It was shown that alloying of Pd with Au provided stabilized bimetallic electrocatalyst for ethanol oxidation [18]. Au-Pd bimetallic nanoparticles supported on tungsten carbide have shown a significant initial potential shift for ethanol oxidation compared to Pt/C electrode [19]. Pd deposited on carbon supported gold nanoparticles [20] as well as on gold nanowires [21] has shown an enhanced catalysis for ethanol reaction, with the positive influence of the gold substrate on palladium deposit due to the electronic effect. Addition of Au on Pd/C electrodes also promotes its activity towards ethanol oxidation [22]. Pd/Au(111) surfaces obtained by the under potential deposition of different amounts of Pd on Au(111) exhibited enhanced catalytic properties for ethanol oxidation compared to pure Au(111) in alkaline media [23].

Compared to Pd/Au bimetallic catalysts obtained by various other methods, Au surfaces modified by spontaneously deposited Pd nanoislands have shown remarkable catalytic properties for both hydrogen evolution and oxygen reduction reactions [24–26]. The improved catalytic performance of such electrodes for cathodic processes was explained by the strong electronic effect of the gold substrate on the deposited Pd islands. It was a challenge to examine the performance of such electrodes on the anodic processes, for which purpose the oxidation of ethanol has been chosen as the test reaction. Moreover, the deposition of palladium was performed using both $PdSO_4 \cdot 2H_2O$ and $PdCl_2$ salts in order to investigate the effect of the counter anion on the morphology and catalytic performance of obtained different Pd/Au(111) nanostructures.

2. EXPERIMENTAL

Au(111) single crystal, 12 mm in diameter, (MaTeck, Julich, Germany), was used as a working electrode and a substrate for Pd deposition. In order to get a clean well ordered crystal, electrochemical

polishing and subsequent annealing in butane flame was performed before each experiment. Electrochemically polished polycrystalline Pd, 5 mm in diameter, disc electrode (Pine Instruments Co.), was used for comparative electrochemical measurements.

Spontaneous deposition was performed by a simple immersion of Au(111) into (2 mM PdSO4·2H$_2$O + 0.05 M H$_2$SO$_4$) or (2 mM PdCl$_2$ + 0.05 M H$_2$SO$_4$) solution at the open circuit potential for the deposition times of 3 and 30 minutes. Au(111) substrate was electrochemically cleaned after each experiment in order to remove Pd deposit.

After each deposition, the obtained Pd/Au(111) nanostructures were characterized *ex situ* using Atomic Force Microscopy (Multimode quadrex SPM with Nanoscope IIIe controller, Veeco Instruments, Inc.) operating in tapping mode under ambient conditions. As described elsewhere [24–26], height AFM images depicting surface topography and phase AFM images sensitive to the surface chemical composition were obtained simultaneously. Coverage was estimated from phase AFM images as the fraction of Au(111) surface covered with the deposited Pd islands, while the degree of the surface chemical modification was qualitatively observed from histograms obtained from the same phase AFM images. Images were acquired from different locations over each electrode surface in order to gain more comprehensive insight into surface characteristics, and to ensure more accurate analysis of observed features. Final image processing was done using Veeco Nanoscope III program, and additionally using WSxM SPM software [27].

Electrochemical characterization of obtained nanostructures and bare Au(111) and Pd(poly) surfaces was performed by cyclic voltammetry (CV) in 1 M NaOH using hanging meniscus method. In separate series of experiments, catalytic properties of Pd/Au(111) surfaces for ethanol oxidation reaction were examined in 1 M NaOH solution with the addition of 0.4 M ethanol. Each CV experiment was preceded with the stabilization of Pd islands to its metallic state by holding the potential for 15 minutes at -0.86 V.

Depositing solutions were prepared with either PdSO$_4$·2H$_2$O or PdCl$_2$ salts supplied by Alfa Aesar, and suprapure H$_2$SO$_4$ (Merck). Working solutions were prepared from NaOH (Merck), ethanol (Merck) and Milli-pure water. In all CV experiments, NaOH solutions were deoxygenated with 99.999 % N$_2$ (Messer). Pt wire and Ag/AgCl, 3M KCl were used as counter and reference electrodes, respectively. All measurements were performed at room temperature.

3. RESULTS AND DISCUSSION

3.1. AFM surface topography and phase images of Pd/Au (111) surfaces

Top-view AFM image (1 x 1) μm^2 of Au(111) substrate surface given in Figure 1 (a), shows surface topography of Au(111) single crystal, consisting of 200 nm up to 500 nm wide terraces separated by steps. Cross section along the line indicated in the image shows one monolayer high (0.24 nm) step and the other step which is three monolayer high, Figure 1 (b). The image indicates that the initial Au(111) surface is clean and well ordered.
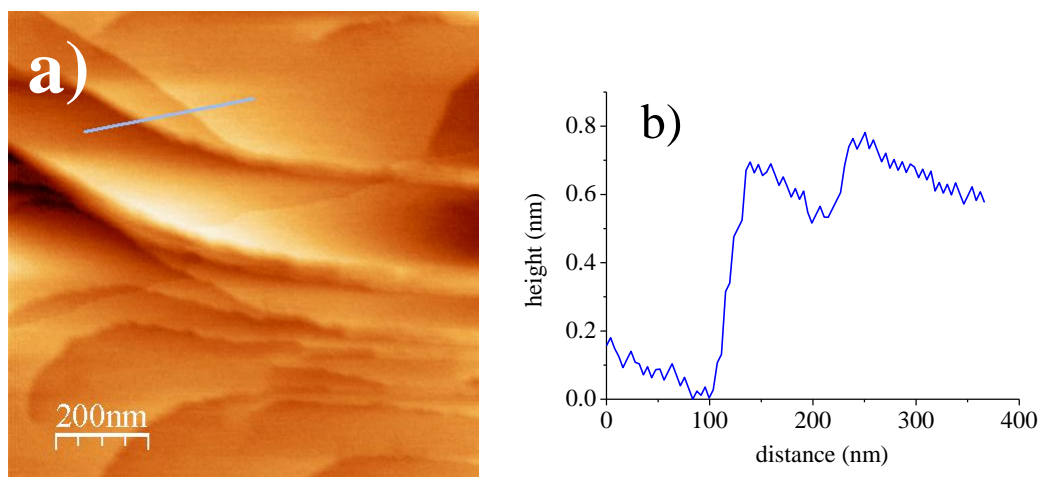
Figure 1. a) Top-view AFM image of the clean Au(111) surface, z-range 1.7 nm; b) cross-section along the line indicated in the image.

AFM height and phase images, sensitive to the surface topography and the changes in the chemical surface composition (coverage), respectively, are acquired for 3 and 30 min Pd deposition from both (2 mM $PdSO_4 \cdot 2H_2O$ + 0.05 M H_2SO_4) and (2 mM $PdCl_2$ + 0.05 M H_2SO_4) solutions. In both cases, when the deposition was performed for 3 min using Pd salt containing either sulfate or chloride as the counter ion, island growth was observed, with a similar coverage of approx. 50 %. In the case when the depositing $PdSO_4$ salt was used, larger and higher randomly distributed islands were obtained, while smaller and thinner islands, showing a pronounced step decoration were observed for $PdCl_2$ salt. Since, these results are very similar to those already reported in refs. [25,26], obtained for longer deposition time and lower concentration of the depositing Pd cations, they will not be presented. Instead, AFM images obtained for 30 min deposition from both $PdSO_4$ and $PdCl_2$ containing solutions, showing higher coverage of the gold surface with Pd islands are presented in Figures 2 and 3, respectively. Besides, the cross–section analyses are also presented, showing the size and shape of the deposited Pd islands, whose influence on the catalysis of ethanol oxidation will be discussed later in this work.

Surface topography and phase AFM images (1 x 1) μm^2 of Pd/Au(111) surfaces, obtained after 30 min Pd deposition using $PdSO_4 \cdot 2H_2O$ salt are presented in Figure 2 (a) and (b), respectively. Surface topography image shows Pd islands randomly distributed over gold substrate, while due to the contrast enhancement in a corresponding phase image, particular Pd islands are clearly highligted. Although Pd islands are not uniform in size with respect to both islands width and height, cross–section analyses, Figure 2 (c) and (d), show that they are mostly 20–40 nm wide and multilayer (0.5–2 nm) high. Pd islands can be clearly distinguished from the underlaying gold substrate, by subtracting lower areas adjusting the treshold at the lowest value in the cross section of the phase image, Figure 2 (e).
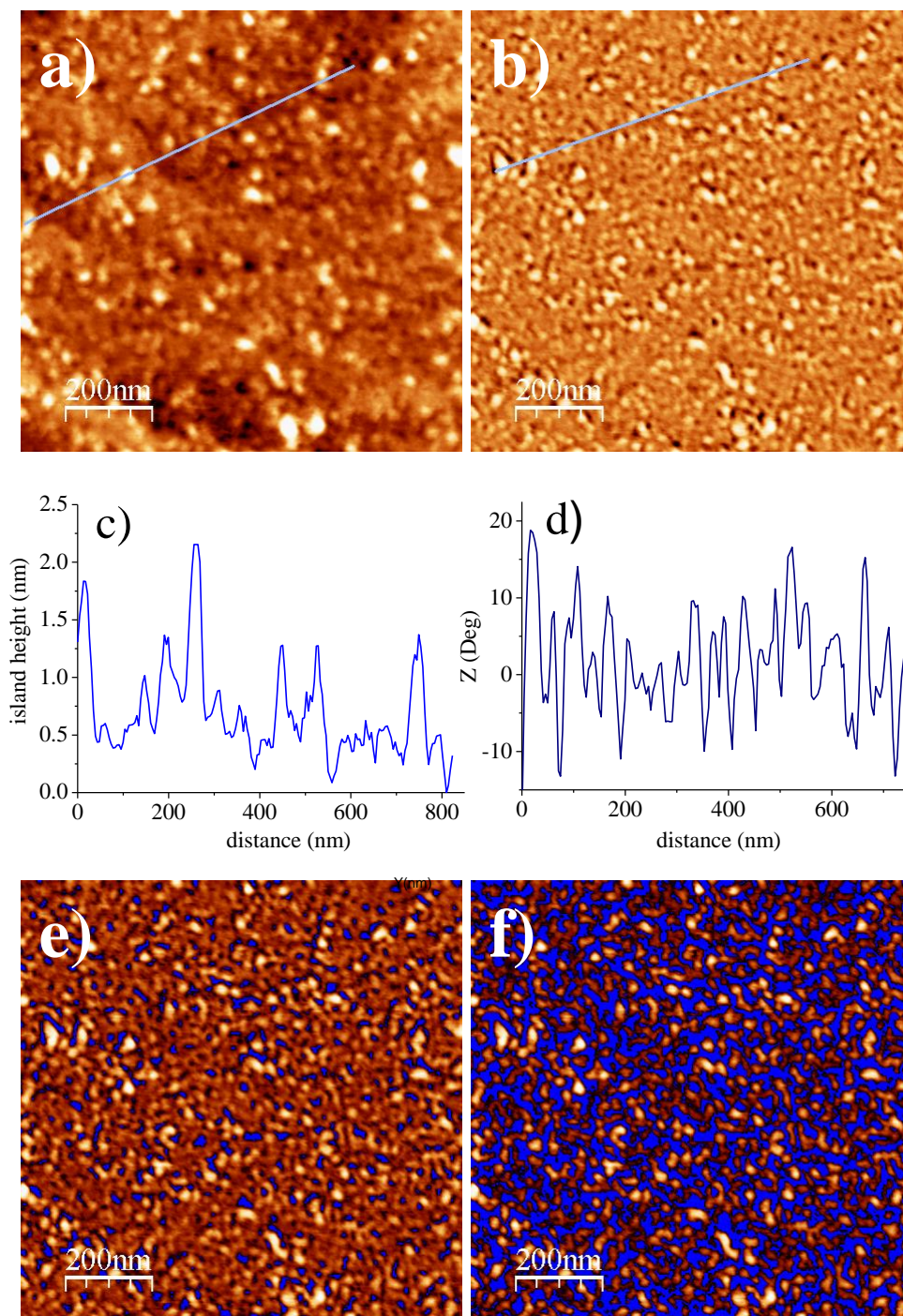
Figure 2. AFM images (1.0 x 1.0) μm^2 of Pd/Au(111) surfaces obtained after 30 min Pd deposition using $PdSO_4 \cdot 2H_2O$ salt, showing: a) surface topography, z-range 3.5 nm; b) corresponding phase image, z-range 39.7°; c) cross section along the line in surface topography image; d) cross section along the line in phase image; e) the overall coverage of 87 % is obtained with the threshold taken at -12 degrees (see d); f) the coverage of higher islands of 56 % obtained when the threshold is set at -2 degrees.

Since phase images are particularly sensitive to the surface chemical composition, this enables quite accurate estimation of the surface coverage, which is taken as a percentage of the gold surface

covered with the deposited Pd islands. The coverage obtained after 30 min Pd deposition was 87 %. When the threshold in phase images was set at the height which corresponded to one Pd monolayer, than the surface coverage which was estimated to be approx. 56 % referred to the islands two or more monolayer high as shown in Figure 2 (f).
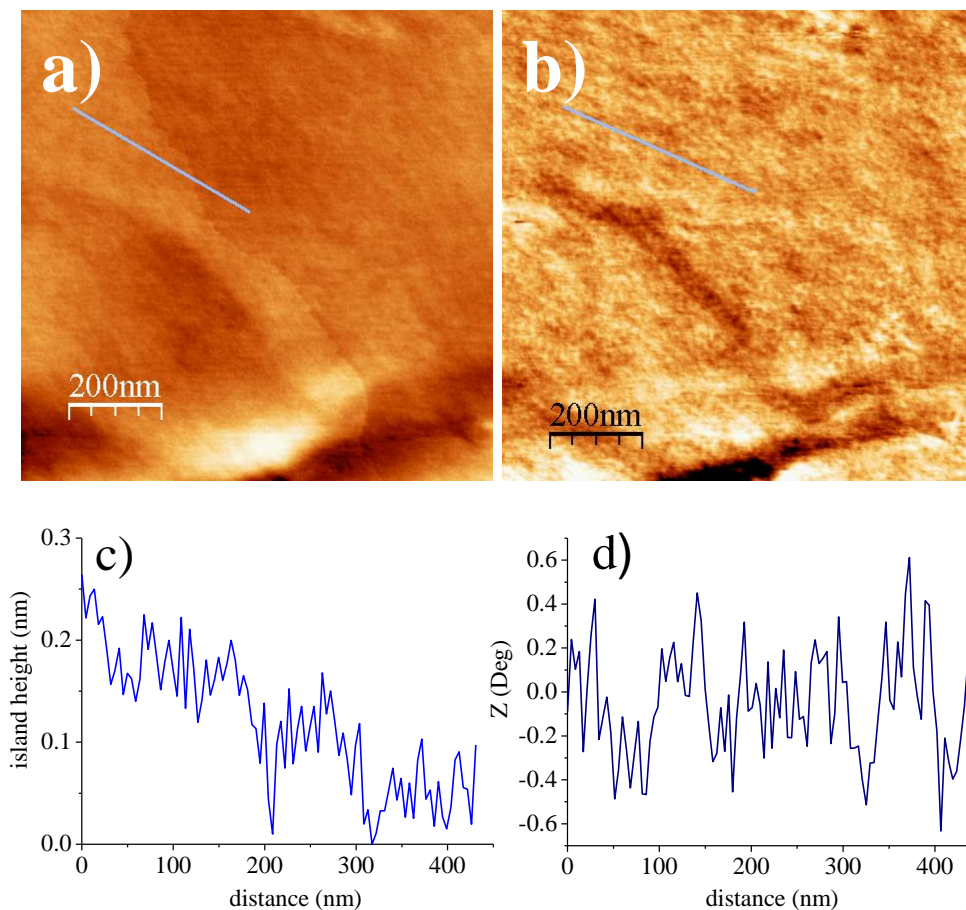

Figure 3. AFM images (1.0 x 1.0) μm^2 of Pd/Au(111) surfaces obtained after 30 min Pd deposition using PdCl$_2$ salt: a) surface topography, z-range 1.3 nm; b) corresponding phase image, z-range 6.2^o; c) cross section along the line in surface topography image; d) cross section along the line in phase image.

Surface topography and phase AFM images (1 x 1) μm^2 of Pd/Au(111) surfaces, obtained after 30 min Pd deposition using PdCl$_2$ salt are presented in Figure 3 (a) and (b), respectively. Images reveal that gold substrate is almost fully covered by Pd layer. Individual islands are mainly monolayer high and 10–20 nm wide, significantly smaller than in the previous case as can be seen in Figure 3 (c) and (d).

Since phase AFM images are sensitive to the elasticity (or hardness) of the material and independent of the topography, phase surface analysis is based on the changes of the histograms of the phase images obtained using Bearing analysis, and which are characteristic for each material [28].

Therefore, positions of the peaks in histograms obtained for Pd/Au(111) can be used to qualitatively detect the changes in surface composition after palladium was deposited using different salts.
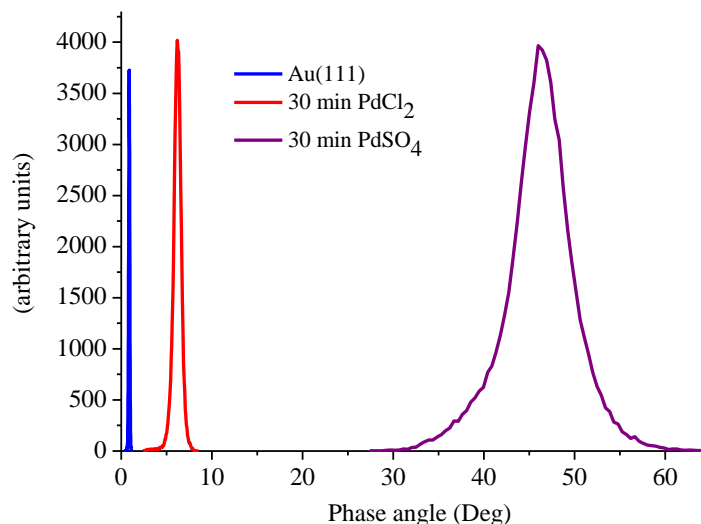

Figure 4. Histograms of phase images illustrating a qualitative change in the surface chemical composition obtained from phase AFM images from Figures 2 and 3. Phase shift with respect to the phase angle for pure Au(111) surface is larger for Pd/Au(111) surface obtained using PdSO$_4$ salt than for one obtained using PdCl$_2$ salt.

Histograms obtained from phase AFM images from Figures 2 and 3, showing a phase shift for Pd/Au(111) surfaces obtained for 30 min deposition from PdSO$_4$ and PdCl$_2$ solutions and compared to the phase angle for the pure Au(111) surface are given in Figure 4. Larger values of the phase angle obtained for Pd/Au(111) surfaces with respect to pure Au(111) may indicate that there has been an increase in the surface elasticity or the decrease in surface hardness. Since palladium is harder than gold, the obtained opposite behavior might be explained by the lower orderliness of the palladium deposit with respect to well ordered Au(111) substrate and/or by the presence of palladium oxides on the gold surface which means that palladium is less strongly bounded to the substrate surface due to its cationic nature. The effect is more pronounced in the case when Pd/Au(111) is obtained using PdSO$_4$ salt than using PdCl$_2$ salt indicating that the later produces more compact Pd layer, strongly bounded to the substrate surface and more metallic.

Although, the coverage estimated from phase images should provide reliable data due to the chemical contrast, it is well known that due to the electronic effect by the gold substrate the active surface area might not be the same. Active surface area of the deposited Pd will be further estimated from cyclic voltammetry curves.

3.2. Cyclic voltammetry curves of Pd/Au(111) surfaces

CV profiles of different Pd/Au(111) nanostructures obtained after 3 and 30 min Pd deposition from both PdSO$_4$·2H$_2$O and PdCl$_2$ salts, as well as CV profiles of the initial Au(111) and bare Pd(poly)

surfaces, all recorded in 1 M NaOH solution, are presented in Figure 5. Voltammetry profile of a clean and well ordered Au(111) surface in alkaline media, given in Figure 5 (a) and (b) is in agreement with the literature data [29]. It is characterized by the first peak at 0.09 V associated with OH-chemisorption, and the second one at 0.30 V associated with AuOH formation. Further oxidation of Au(111) surface occurs at higher potentials. In the reverse sweep, peak at 0.08 V corresponds to the reduction of AuOH. CVs of different Pd/Au(111) nanostructures obtained using $PdSO_4 \cdot 2H_2O$ and $PdCl_2$ salts are also given in Figure 5 (a) and (b), respectively. Starting from the negative potential limit of -1.09 V, the double layer is wider than on pure gold indicating the presence of Pd deposit. The adsorption of hydrogen is pronounced only on Pd/Au(111) surfaces obtained after 30 min deposition using $PdCl_2$ salt which is indicated by the presence of H_{UPD} peaks at -0.9 and -0.5 V. This means that in this case, when thinner and compact palladium deposit is present on the Au(111) surface (see Figure 4), the obtained surface structure geometry is more convenient with respect to palladium surface sites energetically suitable for hydrogen adsorption, which takes place at the potential of -0.5 V corresponding to H_{UPD} on pure Pd as can be seen from Figure 5 (c). It has to be mentioned that at potentials lower than -0.7 V, hydrogen evolution instead of hydrogen adsorption occurs on pure Pd(poly) [30,31]. For all Pd/Au(111) nanostructures, the oxidation of the deposited Pd begins at approx. -0.30 V, like on pure Pd(poly), which at potentials higher than 0.1 V coincides with the oxidation of the substrate Au(111) surface. Peaks associated with the reduction of Pd oxide can be observed in the reverse sweep at approx. -0.2 V, like in the case of Pd(poly), when the positive potential limit is set at the value corresponding to the formation of 1 ML of Pd oxide as can be seen in Figure 5 (c). Reduction peak corresponding to the deposit obtained after 3 min deposition from $PdCl_2$ salt shows a bit higher intensity and wider potential region compared to the deposit obtained after 3 min deposition from $PdSO_4$ salt. In the case of 30 min deposition, deposit obtained using $PdCl_2$ salt exhibited wider reduction peak with lower intensity compared to one originating from $PdSO_4$. Active surface area of Pd islands can be calculated from CVs, as described in ref. [24]. For Pd deposited using $PdSO_4$ salt, estimated active surface areas were 51 % and 85.5 % for 3 and 30 min deposition, respectively. In the case of $PdCl_2$ salt, Pd active surface areas of 53 % and 87 % were calculated for 3 and 30 min deposition, respectively. These results are in agreement with the values estimated from phase AFM images, except for 30 min deposition using $PdCl_2$ salt, for which AFM images reveal full coverage.

3.3. Ethanol oxidation on Pd/Au (111) surfaces

Ethanol oxidation reaction was examined in 1 M NaOH solutions containing 0.4 M of ethanol. Catalytic activities for this reaction of different Pd/Au(111) nanostructures, Au(111), and bare Pd(poly) are comparatively presented in Figure 6. Oxidation peak observed on Au (111) in the positive going scan at 0.15 V, Figure 6 (a) and (b), can be ascribed to the oxidation of adsorbed ethanol molecules, while the one observed in the negative going scan at 0.05 V can be ascribed to the subsequent removal of carbonaceous species that were not completely oxidized in the forward scan.
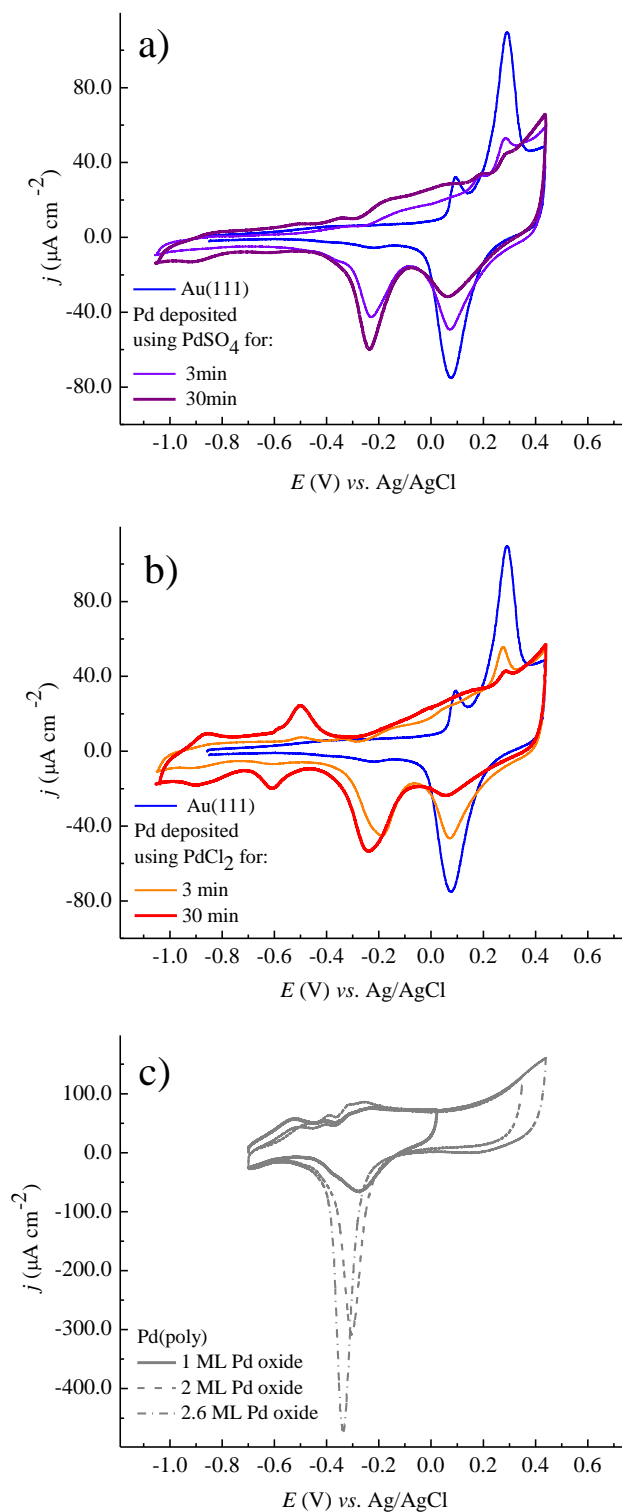
Figure 5. Cyclic voltammetry curves recorded in 1 M NaOH with the potential scan rate of 50 mV s^{-1} of: a) Pd/Au(111) nanostructures obtained using PdSO$_4$·2H$_2$O salt compared to Au(111); b) Pd/Au(111) nanostructures obtained using PdCl$_2$ salt compared to Au(111); c) Pd(poly).

If compared to the CV of Au(111) surface from Figure 5, it can be seen that ethanol oxidation occurs in the potential range of OH⁻ adsorption and AuOH formation only. With the addition of Pd, the initial potential shifts negatively, and falls within the double-layer potential region for pure Au(111). Differences in ethanol oxidation on the initial Au(111) and on different Pd/Au(111) nanostructures can be clearly observed. In both positive and negative going scans, due to the presence of the deposited Pd two ethanol oxidation peaks can be seen on modified gold surface instead of one on pure Au(111) surface. For all Pd/Au(111) nanostructures examined, ethanol oxidation is characterized with the rising of a new current peak in the forward scan at approx. -0.5 V, meaning that the initial potential shifts significantly towards more negative values for approx. 0.4 V with respect to the initial potential for ethanol oxidation on pure gold. The potential where this peak starts to decrease corresponds to the beginning of Pd oxide (or PdOH) formation (see Figure 5). In the reverse scan, a new oxidation peak associated with the deposited Pd arises at the potentials where Pd active sites for ethanol adsorption are liberated due to reduction of Pd oxide [15,32]. It is worth noting that these peaks correspond to ethanol oxidation on pure Pd(poly), Figure 6 (c), although they are slightly shifted towards more positive potentials. Besides, peak corresponding to ethanol oxidation on pure Au(111) is strongly suppressed at all Pd/Au(111) surfaces due to the presence of the deposited Pd islands. It should be noted that surfaces obtained after deposition for 3 min using PdCl₂ and for 30 min using PdSO₄ salt, exhibited the same initial potential for ethanol oxidation, although the current peak densities were higher in the case of 3 min deposition using PdCl₂ salt.

The fact that catalytic properties for ethanol oxidation of all Pd/Au(111) surfaces examined in this work are improved compared to Au(111), but still lower when compared to Pd(poly), indicate that a strong electronic effect of the substrate on the deposit is responsible for the observed catalytic behavior of Pd modified Au(111) surfaces. Furthermore, two peaks for ethanol oxidation, coinciding with the oxidation on Pd (or Pd/Au) sites and Au sites both exhibited lower intensity with respect to the peak intensity on either pure Pd(poly) or pure Au(111). This indicates that Pd/Au(111) surfaces are acting as composed of two different surfaces on which ethanol oxidation is occurring and whose fractions depend on the Pd coverage. In the case of Pd/Au(111) nanostructures obtained using PdSO₄ salt, ethanol oxidation peaks increase, and initial potential shifts towards more negative values with the increase of Pd coverage. In the case of Pd/Au(111) surfaces obtained using PdCl₂ salt, slightly better catalytic properties for ethanol oxidation are obtained for lower Pd coverage. This fact can be explained by the differences in nucleation processes due to different counter anion in Pd salts used for deposition, as will be discussed below.

It is well known that a major problem concerning ethanol oxidation on noble metals is the adsorption of poisoning intermediates, which leads to the deactivation of the electrode surface for further oxidation. Ratio between the intensity of the forward (I_f) and backward (I_b) scan current peaks can be used to evaluate the level of the electrode surface contamination with adsorbed poisoning species. For ethanol oxidation on Au(111), I_b/I_f was calculated to be 0.72, while for Pd(poly) this ratio was 1.86, meaning that Pd(poly) is more prone to poisoning than pure Au(111). For modified surfaces obtained after Pd deposition for 3 and 30 minutes from PdSO₄·2H₂O, I_b/I_f ratios were 0.75 and 0.99, respectively. On the other hand, for Pd/Au(111) nanostructures obtained after Pd deposition for 3 and 30 minutes using PdCl₂ salt, equal values for I_b/I_f ratio of about 0.65 were estimated in both cases.
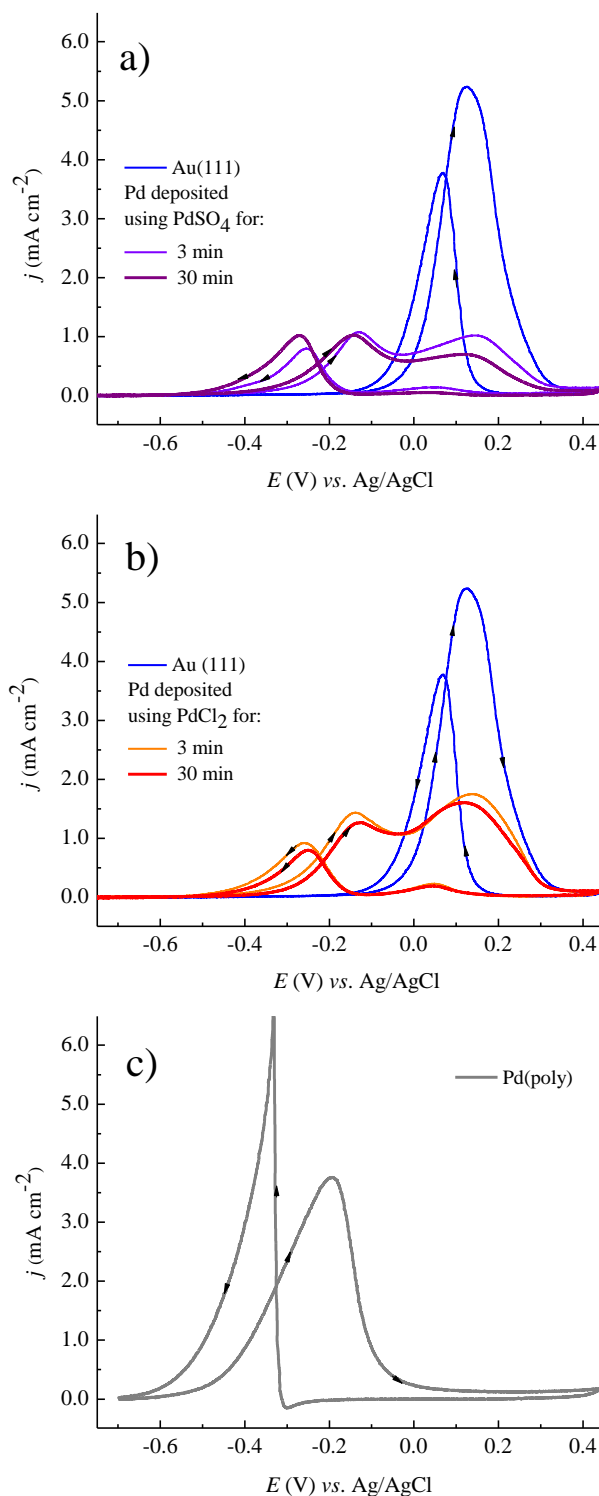
Figure 6. Cyclic voltammetry curves recorded in 1 M NaOH + 0.4 M ethanol with the potential scan rate of 50 mV s^{-1} showing ethanol oxidation on: a) Pd/Au(111) nanostructures obtained using PdSO$_4$·2H$_2$O salt compared to Au(111); b) Pd/Au(111) nanostructures obtained using PdCl$_2$ salt compared to Au(111); c) Pd(poly). Scan direction is indicated by arrows.

The lowering of this ratio for ethanol oxidation on different Pd/Au(111) nanostructures with respect to pure Pd(poly), means that Pd modified Au(111) surfaces are less prone to poisoning. This indicates that the electronic effect of Au(111) substrate on Pd deposit could be responsible for the weakening of bonding interactions between adsorbed species and Pd [25]. Besides, the fact that among different Pd/Au(111) surfaces, the ones obtained using PdCl$_2$ salt, have the lowest I_b/I_f ratio points out to the role of surface morphology where it seems that smoother and thinner Pd deposits are less susceptible to poisoning.

3.4. Comparison of the catalytic effect for ethanol oxidation on different Pd/Au(111) surfaces

Since Pd deposit obtained using PdCl$_2$ salt for 3 min deposition exhibited the highest current density peaks as well as the lowest initial potential for ethanol oxidation, it is compared with the catalytic activity of Pd/Au(111) surfaces obtained for the same deposition time of 3 min using PdSO$_4$·2H$_2$O salt, along with the activity of Au(111) and Pd(poly) as presented in Figure 7.
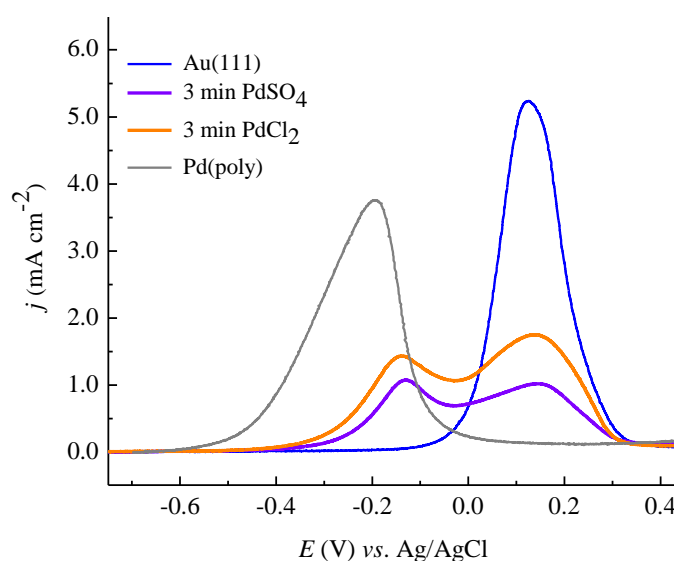

Figure 7. Comparison of the catalytic effect for ethanol oxidation on Pd/Au(111) nanostructures obtained using Pd salts with different counter anions with ethanol oxidation on pure Au(111) and Pd(poly) surfaces in 1 M NaOH solution containing 0.4 M of ethanol. Scan rate was 50 mV/s.

As stated above, the initial potential for modified surfaces is placed between the initial potentials for Pd(poly) and Au(111). Different catalytic effect obtained for different Pd/Au(111) surfaces can be interpreted considering the counter anion from Pd salt. As elaborated in ref. [26], different counter anion in Pd salts affects the rate of the deposition process, and thus the morphology of Pd/Au(111) surfaces. Deposition from PdCl$_2$ is slower and formed Pd islands are smoother and lower, with a preferential step decoration. On the other hand, faster deposition from PdSO$_4$ produced rougher and higher Pd islands randomly distributed over the substrate surface.

It seems that the size and morphology of Pd islands generated from $PdCl_2$ after 3 min deposition are the most convenient for the adsorption of ethanol reactive species and their further oxidation. According to mechanistic studies, ethanol oxidation on Pd in alkaline media starts with the adsorption of ethanol or etoxi (CH_3CHO) species at low potentials, which are further oxidized at higher potentials [15,32]. It can be speculated that the adsorption of ethanol reactive species is more difficult on active sites placed on larger, higher and rougher Pd islands obtained from $PdSO_4$, while it is more convenient to adsorb on smoother, thinner and lower islands produced from $PdCl_2$. If only the deposition from $PdCl_2$ is considered, better catalytic activity for lower Pd coverage can be again explained with more appropriate size and morphology of Pd islands for ethanol adsorption. After considering the electronic effect of the gold substrate on the deposited palladium islands, and the influence of the counter anion from Pd salts on the morphology of the formed deposit, conclusion can be made that the optimal combination of these effects is obtained after 3 min deposition using $PdCl_2$ salt.

4. CONCLUSIONS

Results presented in this paper have shown that Pd/Au(111) nanostructures obtained by spontaneous deposition using different Pd salts ($PdCl_2$ and $PdSO_4 \cdot 2H_2O$) have significantly improved catalytic activity for ethanol oxidation in alkaline media with respect to pure Au(111) surface. AFM analysis revealed that surface morphology including both the size and coverage of the deposited Pd islands was strongly affected by the counter anions in Pd salts used for deposition. In the case when $PdCl_2$ was used, smaller palladium islands mainly monolayer high were obtained, producing thinner and smoother palladium deposit, while in case when $PdSO_4$ salt was used, these islands were larger and higher producing rather rough palladium deposit.

In all cases the oxidation of ethanol on Pd/Au(111) is characterized by the rise of a new peak at approximately the same potential for the same coverage, indicating similar electronic modification of Pd islands by the Au(111) substrate. Pd/Au(111) nanostructures obtained using $PdCl_2$ salts have shown higher ethanol oxidation current densities. This could be ascribed to the surface structure consisting of thinner and smoother palladium deposit which provides more surface sites convenient for the adsorption of ethanol reactive species and their subsequent oxidation.

References

1. Y. Lin, S. Tanaka, *Appl. Microbiol. Biotechnol.* 69 (2006) 627.
2. S.C.S. Lai, S.E.F. Kleijn, F.T.Z. Ozturk, V.C. van Rees Vellinga, J. Koning, P. Rodriguez, M.T.M. Koper, *Catal. Today* 154 (2010) 92.
3. R.B. de Lima, H. Varela, *Gold Bulletin* 41 (2008) 15.

4. G. Tremiliosi-Filho, E.R. Gonzalez, A.J. Motheo, E.M. Belgsir, J.M. Leger, C. Lamy, *J. Electroanal. Chem.* 444 (1998) 31.
5. V. Rao, Hariyanto, C. Cremers, U. Stimming, *Fuel Cells* 7 (2007) 417.
6. S.C.S. Lai, M.T.M. Koper, *Phys. Chem. Chem. Phys.* 11 (2009) 10446.
7. J.R. Varcoe, R.C.T. Slade, *Fuel Cells* 5 (2005) 187.
8. S.Štrbac, M. Avramov Ivić, *Electrochim. Acta* 54 (2009) 5408.
9. K. Ding, H. Yang, Y. Wang, Z.Guo, *Int. J. Electrochem. Sci.* 7 (2012) 4663.
10. S. Yan, L. Gao, S. Zhang, W. Zhang, Y. Li, L. Gao, *Electrochim. Acta* (2013) doi:10.1016/j.electacta.2013.01.087
11. Z.X. Liang. T.S. Zhao, J.B. Xu, L.D. Zhu, *Electrochim. Acta* 54 (2009) 2203.
12. X. Fang, L. Wang, P.K. Shen, G. Cui, C. Bianchini, *J. Power Sources* 195 (2010) 1375.
13. Y. Chen, L. Zhuang, J. Lu, *Chin. J. Catal.* 28 (2007) 870.
14. C. Bianchini, P.K. Shen, *Chem. Rev.* 109 (2009) 4183.
15. S. Sun, Z. Jusys, R.J. Behm, *J. Power Sources* 231 (2013) 122.
16. C. Xu, P.K. Shen, Y. Liu, *J. Power Sources* 164 (2007) 527.
17. B. Pierozynski, *Int. J. Electrochem. Sci.* 8 (2013) 634.
18. J.B. Xu, T.S. Zhao, S.Y. Shen, Y.S. Li, *Int. J. Hydrogen Energy* 35 (2010) 6490.
19. M. Nie, H. Tang, Z. Wei, S.P. Jiang, P.K. Shen, *Electrochem. Commun.* 9 (2007) 2375.
20. L.D. Zhu, T.S. Zhao, J.B. Xu, Z.H. Liang, *J. Power Sources* 187 (2009) 80.
21. S. Cherevko, X. Xing, C-H. Chung, *Electrochim. Acta* 56 (2011) 5771.
22. Y-Z. Su, M-Z. Zhang, X-B. Liu, Z-Y. Li, X-C. Zhu, C-W. Xu, S.P. Jiang, *Int. J. Electrochem. Sci.* 7 (2012) 4158.
23. Z. Dursun, S.U. Karabiberoglu, B. Gelmez, A. Basaran, *Turk. J. Chem.* 35 (2011) 349.
24. I. Srejić, M. Smiljanić, B. Grgur, Z. Rakočević, S. Štrbac, *Electrochim. Acta* 64 (2012) 140.
25. M. Smiljanić, I. Srejić, B. Grgur, Z. Rakočević, S. Štrbac, *Electrocatal.* 3 (2012) 369.
26. M. Smiljanić, I. Srejić, B. Grgur, Z. Rakočević, S. Štrbac, *Electrochim. Acta* 88 (2013) 589.
27. I. Horcas, R. Fernandez, J.M. Gomez-Rodriguez, J. Colchero, J. Gomez–Herrero, A.M. Baro, *Rev. Sci. Instrum.* 78 (2007) 013705.
28. S. Štrbac, M. Nenadović, Lj. Rajaković, Z. Rakočević, *Appl. Surf. Sci.* 256 (2010) 3895.
29. S. Štrbac, R.R. Adžić, *J. Electroanal. Chem.* 403 (1996) 169.
30. G. Denuault, C. Milhano, D. Pletcher, *Phys. Chem. Chem. Phys.* 7 (2005) 3545.
31. M.H. Martin, A. Lasia, *Electrochim. Acta.* 53 (2008) 6317.
32. D.A. Cantane, F.H.B. Lima, *Electrocatal.* 3 (2012) 324